Simulation and characterization of strange attractors in driven diode resonator systems

Z. Su, R. W. Rollins, and E. R. Hunt
Department of Physics and Astronomy, Ohio University, Athens, Ohio 45701
(Received 20 March 1989)

A single diode resonator system is a nonlinear circuit consisting of a series combination of a resistance, an inductance, and a *p-n* junction diode. Driven single diode resonator systems experimentally show the period-doubling route to chaos, while driven coupled diode resonator systems show the quasiperiodic route to chaos. We present a direct comparison of numerical simulations with experimental measurements on driven diode resonator systems. The numerical simulations are based on an extension of the Rollins and Hunt model [Phys. Rev. Lett. **49**, 1295 (1982)] of the diode (ideal diode modified to include a fixed reverse capacitance and a finite reverse recovery time). The extended model allows the reverse recovery time to depend on the forward current of several previous cycles. The model is applied to both the single diode resonator system and a coupled system consisting of two parallel single diode resonators coupled through a series resistance to a sinusoidal generator. In both cases, the numerical simulations show remarkable global agreement with the experimental measurements. The universal scaling behavior of the simulated coupled diode system at the critical line for the quasiperiodic route to chaos is tested by calculating the spectrum of generalized dimensions characterized by the $f(\alpha)$ spectrum. The results show the same $f(\alpha)$ spectrum as obtained for the sine-circle map at the critical line.

I. INTRODUCTION

The response of a driven anharmonic *p-n*-junction diode resonator, composed of a resistance, inductance, and a diode in series with an oscillator, has been found to exhibit several universal scaling behaviors representing particular routes to chaos. For example, the system has been found to exhibit period doubling,[1-3] tangent-bifurcation intermittency,[4] and interior crises.[5] The resistively coupled diode resonator system shows the quasiperiodic route to chaos.[6-8] Early work attributed the period-doubling and chaotic behavior to the nonlinearity introduced by the voltage-dependent capacitance of the varactor. Van Buskirk and Jeffries[6] used a voltage-dependent differential capacitance which included not only a reverse bias term but also a large effective storage capacitance term in forward bias. They show that this model gives reasonable qualitative agreement with experiments.

Hunt[9] reported the results of experiments which clearly showed that, at least for the vast majority of diodes, the nonlinear reverse bias capacitance of the junction is *not* responsible for the chaotic behavior observed in the diode resonator system. When the current passing through a varactor, or power diode, is driven through zero, the diode does not shut off immediately, but continues to conduct for a time called the reverse recovery time. This effect is well known because it is what limits the useful frequency response of these devices. Hunt[9] showed that the rather large reverse recovery time of such diodes was essential for the observed chaotic behavior.

Rollins and Hunt[3] used this result to form a mathematical model of the diode which was very successful in describing the behavior of the single diode resonator. Their model modified the ideal diode by including a forward bias voltage, a constant (voltage-independent) capacitance when in reverse bias, and a reverse recovery time which is proportional to the maximum forward current on the previous cycle. This results in a piecewise-linear model[10] that is exactly solvable in terms of simple analytic functions fit together by appropriate boundary conditions as time proceeds. Rollins and Hunt[3] showed analytically that, over a broad range of typical operating conditions, this solution gave a rigorous one-dimensional map for the sequence of peak forward currents, and numerical calculation showed that the map was unimodal. Hence, the diode resonator system would be expected to follow a patterned route to chaos, in agreement with the universal behavior found in iterated, unimodal, one-dimensional maps.[11]

The large effective storage capacitance suggested by Van Buskirk and Jeffries[6] and the forward-current-dependent reverse recovery time are two ways of attempting to model the same physical characteristics of the diode. However, because a minority carrier diffusion process is responsible for the reverse recovery time of a *p-n* junction, the behavior can be modeled very well by the delay-equation-type description provided by the reverse recovery time model. Furthermore, as pointed out by Hunt and Rollins,[12] the reverse recovery time can be experimentally observed to depend on the forward current of at least two previous conducting cycles. For such diodes, the diffusion process can have a sufficiently long time constant so that the reverse recovery time may depend on the maximum forward currents in several previous cycles.

We describe below an extended reverse recovery time

model of the p-n junction diode, and compare the model calculations with experimental measurements for both a single diode resonator and resistively coupled diode resonator circuits. We show that, for the experimental situation studied, excellent detailed global agreement with experiment is obtained when the maximum forward current of several previous cycles is used to determine the reverse recovery time.

II. *P-N*-JUNCTION MODEL

Rollins and Hunt[3] proposed a simple model for the single diode resonator system containing the minimal properties of the p-n-junction diode responsible for the observed period-doubling bifurcations and chaos, and ignored the other, largely irrelevant, nonlinear properties. This model treats a p-n-junction diode as an ideal diode with the following three additional characteristics.

(i) There is a finite forward bias voltage V_F. The diode will not conduct until the forward voltage drop reaches V_F, and the voltage drop remains at V_F as long as the diode is conducting.

(ii) When the voltage drop is less than V_F, the diode does not conduct but acts as a capacitor with fixed capacitance C.

(iii) When the current is driven through zero, the diode does not shut off immediately, but continues to conduct for a time equal to the reverse recovery time τ_r. The reverse recovery time was taken to depend on the maximum forward current as follows:

$$\tau_r = f(|I_m|) , \tag{1}$$

where

$$f(I) = \tau_m [1 - \exp(-I/I_c)] , \tag{2}$$

$|I_m|$ is the maximum forward current during the conducting cycle, and τ_m and I_c are parameters which describe the particular diode resonator system.

Note that $f(I)$ is proportional to I for $I \ll I_c$, otherwise the functional dependency of f on I is not critical. Rollins and Hunt showed that this model gave a rigorous one-dimensional, unimodal map for the sequence of peak forward currents exhibiting the universal period-doubling route to chaos expected of systems described by such maps.

Hunt and Rollins[12] noted that measurements of the sequence of peak forward currents do not result in a rigorous one-dimensional map. Their measurements also indicated that the reverse recovery time actually depends on the maximum forward current during at least the last *two* cycles. An extension of the reverse recovery time model to include a dependence on the peak forward current in the two previous cycles showed much better detailed agreement with the experimental measurements.[12] The model described and used in this paper is a further extension to include the effects of three, or more, previous cycles.

We briefly review the transient properties of a p-n-junction diode[13,14] in order to point out the physical processes which are the basis for the extended model. We assume for this discussion that the forward current is carried predominantly by holes, as would be the case if the n region were lightly doped and the p region heavily doped. Under forward bias, a large excess hole concentration is injected into the n region, where the holes are minority carriers. The injected holes diffuse away from the junction because of a concentration gradient. As they diffuse they combine with the majority carriers, the electrons, so that far from the junction the hole concentration is that normally found in the n region. The average time that an excess minority carrier exists in the diffusion process is called the lifetime τ_p of the minority carriers. When the bias of the junction is reversed, some of the excess minority carriers diffuse back through the junction and supply a reverse current.

The transient behavior of the junction, as the diode shuts off, can be roughly divided into two steps. In the first step, called the recovery phase, the excess hole concentration at the junction surface in the n region is large enough to supply a reverse current determined by the applied voltage and the external resistance in series with the diode. The voltage across the junction during this phase remains roughly the same as under forward bias. The duration of the recovery phase is modeled by our reverse recovery time. It must be noted that the recovery time, as defined here, not only depends on the junction characteristics, but also depends on external circuit parameters such as the series resistance in the circuit. Under steady-state conditions, it can be shown[15] that both the density of excess minority carriers at the junction surface and the net excess minority charge in the n region are proportional to the forward current. This is a partial justification for the form of our function $f(|I_m|)$, defined in Eq. (2), with its linear dependence on $|I_m|$ for small $|I_m|$. In the second step, called the reverse phase, the concentration of excess holes at the junction surface has dropped to zero. The reverse current is supplied by the diffusion of the excess holes deeper in the n region. Thus the reverse current decays rapidly, the resistance of the junction increases greatly, and the voltage across the junction drops abruptly through zero and reverses. As the junction voltage increases in the reverse direction, a space-charge layer is built up in which the free carriers are depleted. Hence under reverse bias the junction behaves as a capacitance whose value depends on the junction voltage.

Consider such a junction driven by a periodic voltage. If the lifetime of the minority carriers is much longer than the period of the drive voltage, and the reverse current is not very large, then the concentration of excess minority carriers may not totally vanish throughout the n region during the reverse phase. This residual concentration of excess minority carriers will reduce the diffusion rate for next forward injection and a cause a higher concentration of excess minority carriers near the junction surface, thus causing a slightly longer reverse recovery time. Several previous cycles may make contributions to the residual concentration of the excess minority carriers if the total time is less than, or comparable to, the lifetime of the minority carriers. The reverse recovery time

model used here is a gross simplification of the actual p-n junction, but it captures the essence of the transient behavior expected.

Thus, following Hunt and Rollins,[12] we extend the model by replacing Eq. (1) with an expression for the recovery time $\tau_{r,n}$ in the nth cycle:

$$\tau_{r,n}=f(|I_m|_n)+\alpha_1 f(|I_m|_{n-1})+\cdots+\alpha_k f(|I_m|_{n-k}) , \tag{3}$$

where $|I_m|_n$ is the magnitude of the peak forward current during the nth cycle, $f(\cdot)$ is the function defined by Eq. (2), and α_k is a parameter for a particular diode resonator system, describing the influence of the kth previous cycle on the reverse recovery time.

The particular diodes used in the work reported here were a 1N1221 for the single diode resonator and two 1N2858s for the double resonator circuit. These Si p-n-junction rectifiers have a measured minority-carrier lifetime of about 100 μsec,[12] while the driving period is only 10–20 μsec. In fact, we found it necessary to include up to three previous cycles and to adjust the weight factors α_1, α_2, and α_3. This procedure allowed us to obtain calculated return maps yielding remarkable detailed agreement with the experimental measurements on the diode resonator systems described below.

III. RESULTS AND DISCUSSION

A. Single p-n-junction diode resonator

1. Implementation of the model

The single p-n-junction diode resonator is composed of a resistance, inductance, and a diode in series with an oscillator. The model described above leads to piecewise-linear equations as described in Ref. 3. The analytic solutions are fit together with appropriate boundary conditions using the step-by-step procedure described in Ref. 3, with the one modification that the reverse recovery time is determined by Eq. (3) instead of Eq. (1). The sequence of maximum forward-current values were calculated from the model and the weight factors α_1, α_2, and α_3 were adjusted to give good qualitative agreement with experimental measurements over a broad range of the drive voltage amplitude. Adjusting the values of α_1, α_2, and α_3 changes the detailed structure of the calculated return maps, $|I_m|_{n+1}$ versus $|I_m|_n$, while leaving the general behavior unchanged. This is consistent with our experimental observations that any diode selected from a box of 1N1221s will give the same general experimental behavior but the details differ from one diode to the next.

2. Comparison with experiment

Hunt and Rollins[12] used a similar model but set $\alpha_k=0$ for $k>1$. When carefully comparing the calculated map shown in Ref. 12 with the measured map shown in the same reference, one finds that the subbranch on the calculated map is on the wrong side of the main branch. We found that to put the subbranch in the correct position it was necessary to include small, nonzero, values for α_2 and α_3.

Figure 1 shows the corresponding calculated (left) and experimental (right) return maps $I(n+1)$ versus $I(n)$ where $I(n)\equiv|I_m|_n$. The experimental data were taken directly from an oscilloscope, as described in Ref. 12. The weight values used in the simulations were $\alpha_1=0.40$, $\alpha_2=0.12$, and $\alpha_3=0.02$. The amplitude of the drive voltage for Fig. 1(a) placed the system in the chaotic state below the period-three window. For the simulation, $V_0/V_F=6.2$ and the corresponding drive voltage for the experiment was $V=2.4$ V_{rms}. The other parameters for the simulation model and the real circuit were the same as defined and used in Ref. 12. The simulation in both Fig. 1(a) and 1(b) contains 1500 calculated points.

Figure 1(b) shows a similar pair of calculated and measured return maps where the drive voltage placed the system in a chaotic state above the period-three window. The parameters for Fig. 1(b) are the same as for Fig. 1(a), except that the drive voltage is larger. For the calculated map $V_0/V_F=9.4$ and for the measured map $V=3.6$ V_{rms}.

The agreement between the calculated and measured return maps is very good and the α_k values seem reasonable in magnitude and decline as k increases, as expected. Increasing the relative contributions from α_2 and α_3 has

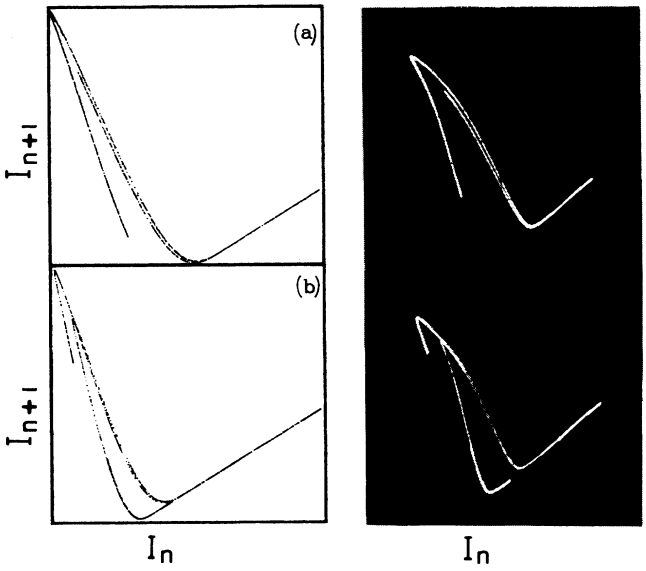

FIG. 1. Corresponding calculated and measured return maps of the peak forward currents of the single resonator in arbitrary units. The simulation data are on the left and the corresponding measurements from the real system are the oscilloscope photographs on the right. (a) The drive voltage used places the system in a chaotic state below the period-three window. Note that the subbranch on the calculated map is in the correct position. (b) A higher drive voltage places the system in a chaotic state above the period-three window.

the effect of widening the spacing between the branches of the map. Furthermore, we found a nonzero value for α_3 was necessary. If α_3 was set to zero, then the subbranch of the calculated map could not be made to fall on the correct side of the main branch by adjusting α_1 and α_2. The success of the extended reverse recovery time model suggests that chaos in the diode resonator system is due to a delayed feedback mechanism provided by the slow diffusion and long lifetime of the excess minority carriers near the junction.

B. Coupled *p-n*-junction diode resonator

1. Implementation of the model

The coupled diode resonator system consists of two parallel, single diode resonators coupled through a series resistance, driven by a sinusoidal voltage, as shown in Fig. 2. This system has been observed experimentally to exhibit a quasiperiodic transition to chaos.[6–8] We applied the extended reverse recovery time model to this system, as described below.

The coupled diode resonator system shown in Fig. 2 was described by the following set of differential equations:

$$L\frac{di_1}{dt}=V_0\cos\theta-V_1-R(i_1+i_2)\ ,$$

$$L\frac{di_2}{dt}=V_0\cos\theta-V_2-R(i_1+i_2)\ ,$$

$$\frac{dV_1}{dt}=\begin{cases}0, & \text{when diode 1 is conducting}\\ i_1/C_1, & \text{when diode 1 is nonconducting}\end{cases}$$

$$\frac{dV_2}{dt}=\begin{cases}0, & \text{when diode 2 is conducting}\\ i_2/C_2, & \text{when diode 2 is nonconducting}\end{cases}$$

$$\frac{d\theta}{dt}=\omega\ ,$$

where the drive voltage $E(t)=V_0\cos(\omega t)$, and i_1, V_1, C_1 and i_2, V_2, C_2 are the current through, voltage across, and reverse capacitance of diodes 1 and 2, respectively. L and R are the inductances and resistance shown in Fig. 2.

The rules for deciding when the diodes are in the conducting state were obtained from the model described in Sec. II and are briefly listed below.

(a) A diode will not enter the conducting state until the forward voltage drop reaches V_F from below.

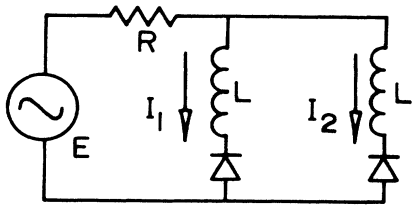

FIG. 2. Circuit diagram used to model the resistively coupled diode resonator system.

(b) A diode will continue in the conducting state for a time τ_r after the current is driven through zero from the forward to the reverse direction. The delay time $\tau_{r,n}$ in the nth cycle is determined by Eqs. (2) and (3) with $k=2$. The same parameter values of α_1, α_2, τ_m, and I_c were chosen for each diode. The only difference in the diodes was reflected by the difference in the capacitances C_1 and C_2 for the diodes in the nonconducting state.

The system of equations are piecewise linear and can be solved analytically, but matching the boundary conditions at the switching time for each diode is algebraically very difficult. Instead, we found it more convenient to solve them by numerical integration. We used a combination of a fourth-order Runge-Kutta method and a Hamming predictor-corrector method. The method was checked by solving the single diode resonator problem and comparing the results with those obtained by fitting together the exact analytic solutions, as described in Ref. 3. We also did numerical checks on the method by using only the slower Runge-Kutta method and comparing the results.

As the numerical integration proceeds, the current and voltage of each diode is monitored to determine when the conducting state of each diode is to be changed. Each time the state of a diode changes, the set of equations used are changed accordingly and the integration process restarted using the current and voltage values at the switching time as initial conditions. The Runge-Kutta method is used to start and stop the Hamming predictor method, which is used between switching times. The procedure is straightforward, although tedious. The procedure was speeded up greatly by using a technique introduced by Hénon[16] to find quickly an accurate estimate of the time at which the current goes through zero, and to find the maximum forward current during each conduction cycle. For example, to get a precise estimate of the time when the current i_1 goes through zero on the way to shutting off, we first determine the time step t_i where i_1 first goes through zero. Then, the roles of i_1 and t are interchanged, making i_1 the independent variable and $t(i_1)$ a dependent variable, and the integration is then stepped back in a single step $\Delta i_1=i_1(t_i)$ to the exact point where $i_1=0$ and the value of t at this point is determined. A similar technique is used to obtain the peak forward current during each conducting cycle for each diode. The sequence of peak forward currents is saved for each diode. Having found the time at which the forward current reached zero for a particular diode, as described above, the delay time τ_r is calculated using Eq. (3) and the saved values of the peak forward currents. That diode will shut off (and the equations will change) at time τ_r after the forward current reaches zero, and the equations are integrated until the known shutoff time is reached. If at shutoff time the current is still in the revese direction, the integration is stopped and the equations are changed to reflect the fact that the diode has shut off. The integration is restarted using the values of all variables at shutoff time as the starting values. Once a diode is off, its voltage drop is monitored until it reaches the forward bias voltage V_F. The Hénon method is used

again to obtain an estimate, in essentially one integration step, of the time at which the voltage reached the forward bias value. At this time the equations are changed to reflect the fact that the diode has turned back on and the integration restarted. And so the process proceeds for each diode.

The values given the system parameters are discussed in terms of reduced quantities defined as in Ref. 3 for the single diode resonator. We define $C=\max(C_1,C_2)$, $\omega_0=1/\sqrt{LC}$, $\nu=\omega/\omega_0$, and $Q=\omega_0 L/R$. The value of Q for the experimental system can be roughly measured. In the case reported here, the coupling resistance R is about 3 kΩ. For each diode resonator the inductance L used is about 100 mH, and the measured resonant frequency is around 50 kHz when the diodes are not conducting. Thus the Q value is estimated to be about 11. We set $Q=10$ for the simulation. The parameters used to determine the delay time τ_r were $\tau_m=0.45(2\pi/\omega_0)=0.45T_0$, and $I_c=1.0V_F/R$. The weighting factors $\alpha_1=0.25$ and $\alpha_2=0.08$ were used. The values of α_k were smaller than those used for the single diode resonator system because larger values of L, R, and T (where T is the period of the drive voltage) were used for the coupled diode resonator system. We found that if we chose $C_1=C_2$ the simulation had more symmetry than the measured system. We found that $C_1/C_2=1.15$ gave better agreement with the results from the measured system.

The simulation of the resistively coupled diode resonator system was carried out using the parameter values given above and the sequences of peak forward currents $I_1(n)$ and $I_2(n)$ were recorded for various values of the reduced drive voltage V_0/V_F. A comparison of the results with experimental measurements is given in Sec. III 2.

2. *Comparison with experiment*

Over a range of drive frequencies, the response of the real and model resistively coupled diode resonator systems were found to show the same global behavior. As the amplitude of the drive voltage is increased, at fixed drive frequency, the response of the system is observed to progress through a series of bifurcations. At low drive voltage, the system starts with a periodic response at the

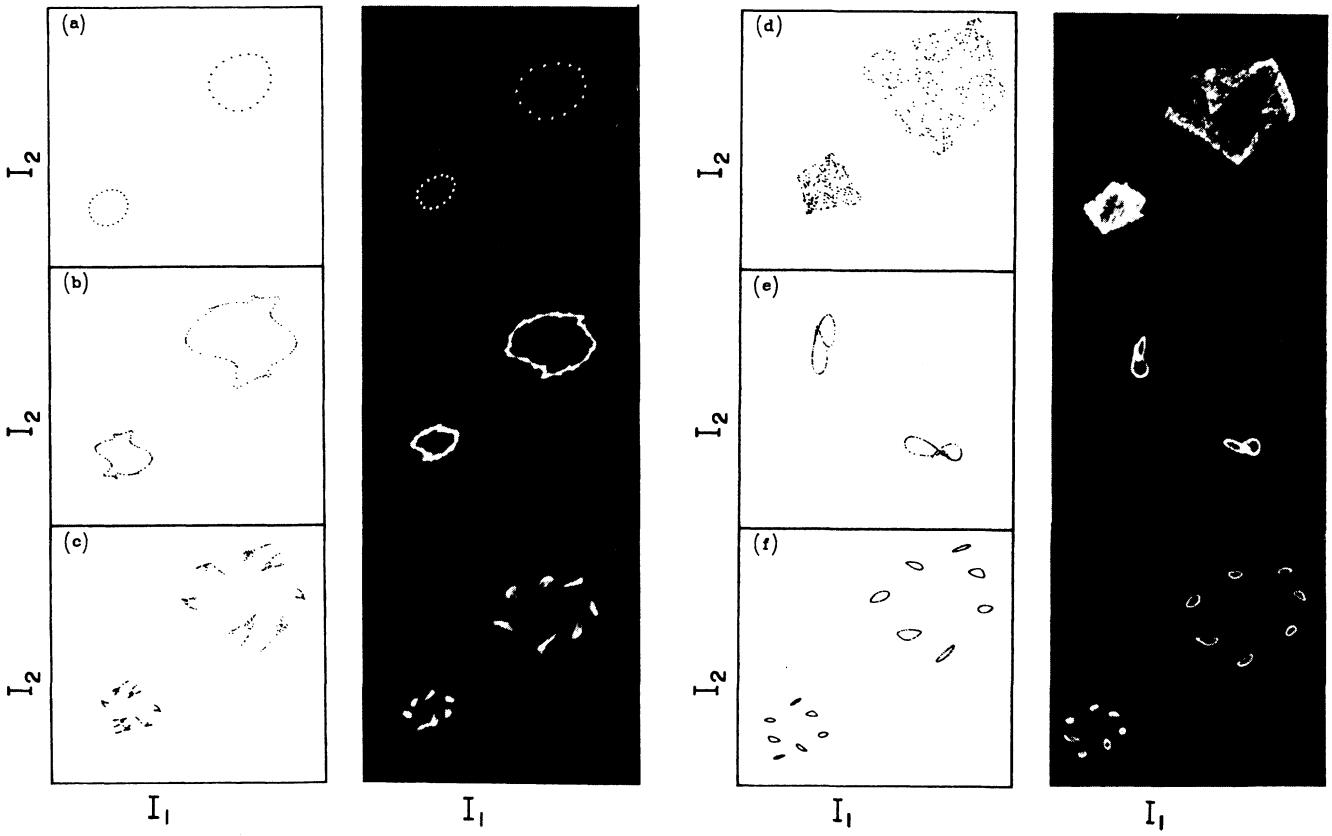

FIG. 3. Corresponding simulated (left) and measured (oscilloscope photographs on the right) Poincaré sections formed by the peak forward currents I_2 vs I_1 (plotted in arbitrary units) for the coupled diode resonator system. The simulations contain 500 calculated points. The drive voltages for the simulation, V_0/V_F, and experimental systems, respectively, were (a) 4.65 and 2.078 V_{rms}, (b) 5.25 and 3.082 V_{rms}, (c) 5.55 and 3.296 V_{rms}, (d) 5.95 and 3.747 V_{rms}, and (e) 6.50 and 4.833 V_{rms}. For (a)–(e), simulation: $\omega/\omega_0=1.30$; measurements: drive frequency, $f=56$ kHz and $R=2940$ Ω. For (f) simulation: $\omega/\omega_0=1.27$, $V_0/V_F=5.29$; and measurements: $f=52.4$ kHz, $R=2964$ Ω, and $V=4.34$ V_{rms}. All other parameters are constant and given in Sec. III B 1.

drive period. The response of the system is observed to period double as the drive voltage is increased and then undergo a Hopf bifurcation where a second frequency spontaneously appears. Mode-locked states, where the ratio of the two frequencies is rational, and quasiperiodic states, where the ratio of the two frequencies is approximately irrational, are observed. As the drive voltage is increased further, a transition to chaos occurs. Chaotic bands, periodic windows, and, finally, reverse bifurcations are all observed in both the real and simulated systems.

Figure 3 shows several Poincaré sections formed by plotting the peak forward currents $I_1(n)$ versus $I_2(n)$ at several values of the drive voltage; all other parameters remain fixed. The results obtained from the simulated and real systems are displayed side by side. The parameter values used for the simulation are those listed in Sec. III 1. The drive frequency in the simulation was fixed at $\omega/\omega_0=1.30$ for Fig. 3(a)–3(e), while the simulation drive voltage ranged from $V_0/V_F=4.65$ in Fig. 3(a) to $V_0/V_F=6.50$ for Fig. 3(e). Each plot of data calculated from the simulation contains 500 points.

The corresponding measured Poincaré sections in Fig. 3 are photographs taken directly from an oscilloscope displaying the peak forward currents $I_1(n)$ versus $I_2(n)$, using measurement techniques described in Ref. 8. The measured Poincaré sections shown in Fig. 3(a)–3(e) were taken from a resistively coupled system with the coupling resistance equal to 2940 Ω, drive frequency fixed at 56 kHz and drive voltage ranging from 2.078 V_{rms} for Fig. 3(a) to 4.833 V_{rms} for Fig. 3(e). The resemblance of the Poincaré sections obtained from the simulation to those measured from the real system is striking, including much of the detailed structure.

At a drive voltage much lower than that used for Fig. 3(a), the Poincaré section is a single point. As the voltage is increased the period doubles and the Poincaré section becomes two points. Then a Hopf bifurcation occurs where the two points open into two circles. Figure 3(a) was obtained at this point with the ratio of the spontaneous frequency to the drive frequency very close to a rational number, so that the Poincaré section is a set of points. Figure 3(b) was obtained when the system is near the critical line for the quasiperiodic transition to chaos, where the real system has been shown to display universal scaling for which the circle map is the paradigm.[7,8] For drive voltages above the critical line, the Poincaré sections of the toroidal attractor break up. Mode locking (periodicity) is observed and the mode-locked states are observed to undergo a second Hopf bifurcation where each point opens into a small circle. Figure 3(c) shows a set of these cross sections of a torus which has just broken into chaos. Figure 3(d) is a chaotic state and Fig. 3(e) a quasiperiodic state which occurs at high drive voltage. Note that the relative position of the two cross sections of the toroidal attractor shift in going from Figs. 3(d) to 3(e). This shift occurs suddenly as the drive voltage is continuously increased. It should be noted that the system is strongly hysteretic once the drive voltage exceeds the critical value for the quasiperiodic transition to chaos. For example, once the system jumps into the attractor shown in Fig. 3(e), it remains in that state, if the drive voltage is reduced, until the system finally jumps back into the period-two attractor observed at low drive voltage before the (first) Hopf bifurcation.

Finally, Fig. 3(f) demonstrates the particularly good correspondence between the simulation and the real system. Here the system was in a mode-locked period-14 (doubled period-7) state which has undergone a (second) Hopf bifurcation, i.e., in the 3/14 region of the phase diagram shown in Fig. 3 of Ref. 8. The size, shape, and position of the small circles are in remarkable agreement.

The rather detailed global agreement demonstrated above leaves little doubt that the simulation model reproduces the main features of the dynamics of the real coupled diode resonator system.

3. *Calculation of $f(\alpha)$ at the critical line*

The spectrum of singularities of strength α, $f(\alpha)$, gives a detailed description of the fractal nature of the entire attractor and is expected theoretically to be a universal function for the quasiperiodic route to chaos.[17] We have reported measurements of the $f(\alpha)$ spectrum for the real coupled diode resonator system at the critical quasiperiodic orbit.[7,8] It is usual to test universal scaling by using the quasiperiodic orbit with an irrational winding number equal to the golden mean [in continued fraction notation: $\langle 1111\ldots\rangle=(\sqrt{5}-1)/2$]. However, our system does not respond at the golden-mean winding number,[7,8] so instead we choose a closely related irrational number $\langle 4111\ldots\rangle=2/(7+\sqrt{5})=0.216\,542\ldots$ at which both the real and simulated coupled diode resonator systems will respond. The critical quasiperiodic orbit with the system's winding number $W=0.216\,542$ was located by carefully adjusting the simulated drive voltage V_0/V_F and drive frequency ω/ω_0 using methods similar to those described in detail in Ref. 8. The values of the other simulation parameters were the same as those used to obtain the results reported in Sec. III B 2.

At the critical orbit the Poincaré section formed by the peak forward currents (I_1,I_2), as described in Sec. III B 2, was obtained. Because the Hopf bifurcation and quasiperiodicity is preceded by a period doubling, the Poincaré sections show two cross sections of a torus, i.e., two circlelike structures, as shown in Fig. 3. Points are visited alternately on the two cross sections. The $f(\alpha)$ spectrum was calculated from data collected from the larger of these two cross sections, and in the discussion which follows we are considering only the sequence of peak currents (I_1,I_2) which lie on this distorted circle.

Figure 4 shows the Poincaré section data from the simulation and the oscilloscope photograph of the corresponding real system. In calculating the simulated orbits, the system of equations were first integrated for 800 drive cycles, to assure transients have disappeared, then the peak forward currents I_1 and I_2 in the next 5634 drive cycles were saved. This allowed us to collect a data set for (I_1,I_2) on the large distorted circle consisting of 2817 points. The peak currents were determined by requiring the derivative $dI/dt=0$ to within 10^{-11} and, including integration errors, we believe the accuracy in I_1 and I_2 to

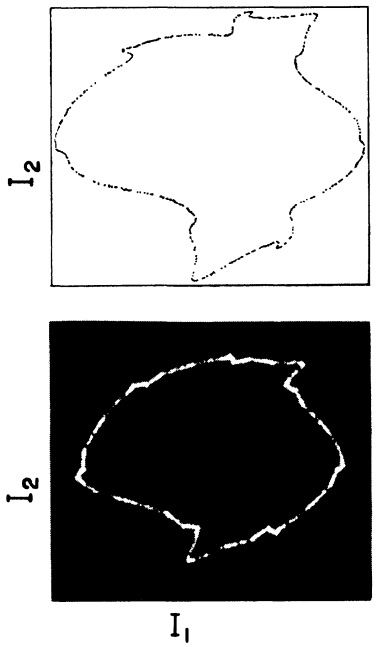

FIG. 4. Corresponding simulated (top) and measured (oscilloscope photograph at the bottom) Poincaré sections at the best approximation to the critical orbit at the transition from quasiperiodicity to chaos with winding number $W=0.216\,542\,4$.

be of the order of a part in 10^{-7} or better.

The winding numbers on the simulated orbit were obtained using the same method which we used for the real system.[8,18] The sequence of peak currents from one of the diodes, say I_1, is plotted versus θ generated by the simple twist map; $\theta_{n+1}=(\theta_n+\Omega)\text{mod}\,1$. The value of Ω is adjusted until a thin line is obtained (for example, see Fig. 5, Ref. 8). The winding number for the simulated orbit could be determined to an accuracy of 2×10^{-7}. By carefully adjusting the simulated drive voltage and drive frequency, the best approximation of the critical orbit with winding number $W=0.216\,542$ was obtained when $V_0/V_F=5.228\,52$ and $\omega/\omega_0=1.297\,92$. The resulting Poincaré section shown at the top of Fig. 4 looks very similar to the corresponding Poincaré section obtained for the real system shown in Fig. 4 of Ref. 8. It is possible to adjust the simulation parameter values Q, C_1/C_2, τ_m, α_1, α_2, and I_c to obtain an orbit with a shape more similar to the measured orbit. However, adjusting these parameters and then finding the critical orbit requires a large amount of computer time. Instead, we adjusted the coupling resistance, drive frequency, and voltage of the real system and located the critical orbit with winding number $W=0.216\,542$, which gave a better match to the shape of the simulated Poincaré section. The oscilloscope photograph showing the corresponding Poincaré section obtained with $R=3600\ \Omega$, $f=67.6$ kHz, and $V=2.98\ V_{\text{rms}}$ is the bottom half of Fig. 4. The shape of the simulated and real orbits are very similar.

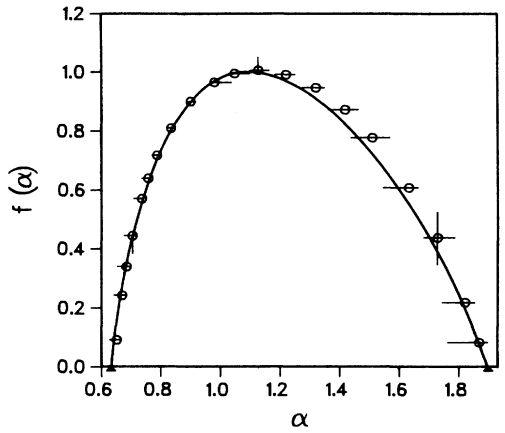

FIG. 5. Calculated $f(\alpha)$ spectrum for the simulated orbit shown at the top of Fig. 4. The solid curve is obtained from the sine-circle map using the same winding number. The endpoints, denoted by solid triangles, are determined theoretically and are the same as found for the golden mean winding number. The error bars are estimates of the accuracy of the $f(\alpha)$ calculation as described in Ref. 8.

The $f(\alpha)$ spectrum was calculated using the same methods used for the real system described in detail in Ref. 8. The results are shown in Fig. 5. The solid curve is obtained from the sine-circle map. The $f(\alpha)$ spectrum strongly supports the experimental results[7,8] and is in good agreement with the theoretical conjecture.[17]

IV. SUMMARY

We have presented a detailed comparison of results obtained from a simulation and those obtained from the corresponding real system for both a driven single diode resonator and for a driven coupled diode resonator system. The excellent detailed global agreement obtained in all cases suggests the extended reverse recovery time model of the *p-n* junction, which was used in the simulations, provides a good description of the essential physical mechanism responsible for the observed chaotic behavior in driven diode resonator systems. In particular, we obtained the excellent agreement by letting the reverse recovery time of the *p-n*-junction diode depend on the peak forward current of several previous conducting cycles. The success of this model suggests that driven diode resonator systems exhibit chaotic behavior because of a delay feedback effect related to the slow diffusion and long lifetime of the excess minority carriers near the *p-n* junction of the diode.

ACKNOWLEDGMENTS

We acknowledge S. Ulloa for many stimulating discussions during the course of this work and T. Tigner for technical assistance.

[1]P. S. Lindsay, Phys. Rev. Lett. **47**, 1349 (1981).
[2]J. Testa, J. Perez, and C. Jeffries, Phys. Rev. Lett. **48**, 714 (1982).
[3]R. W. Rollins and E. R. Hunt, Phys. Rev. Lett. **49**, 1295 (1982).
[4]C. Jeffries and J. Perez, Phys. Rev. A **26**, 2117 (1982).
[5]R. W. Rollins and E. R. Hunt, Phys. Rev. A **29**, 3327 (1984).
[6]R. Van Buskirk and C. Jeffries, Phys. Rev. A **31**, 3332 (1985).
[7]Z. Su, R. W. Rollins, and E. R. Hunt, Phys. Rev. A **36**, 3515 (1987).
[8]Z. Su, R. W. Rollins, and E. R. Hunt, preceding paper, Phys. Rev. A **40**, 2689 (1989).
[9]E. R. Hunt, Phys. Rev. Lett. **49**, 1054 (1982).
[10]For an earlier experimental example of a coupled (tunnel-diode) oscillator system exhibiting chaos and successfully described by a piecewise-linear model, see J. P. Gollub, E. J. Romer, and J. E. Socolar, J. Stat. Phys. **23**, 321 (1980).
[11]M. J. Feigenbaum, Los Alamos Theoretical Division Annual Report No. LA06816-PR, 1977 (unpublished); Physica D **7**, 16 (1983).
[12]E. R. Hunt and R. W. Rollins, Phys. Rev. A **29**, 1000 (1984).
[13]James J. Brophy, *Basic Electronics for Scientists,* 4th ed. (McGraw-Hill, New York, 1983).
[14]Jacob Millman, *Microelectronics, Digital and Analog Circuits and Systems* (McGraw-Hill, New York, 1979).
[15]Jacob Millman, Ref. 14, p. 44.
[16]M. Hénon, Physica D **5**, 405 (1982).
[17]T. C. Halsey, M. H. Jensen, L. P. Kadanoff, I. Procaccia, and B. I. Shraiman, Phys. Rev. A **33**, 1141 (1986).
[18]J. Stavans, Phys. Rev. A **35**, 4314 (1987).

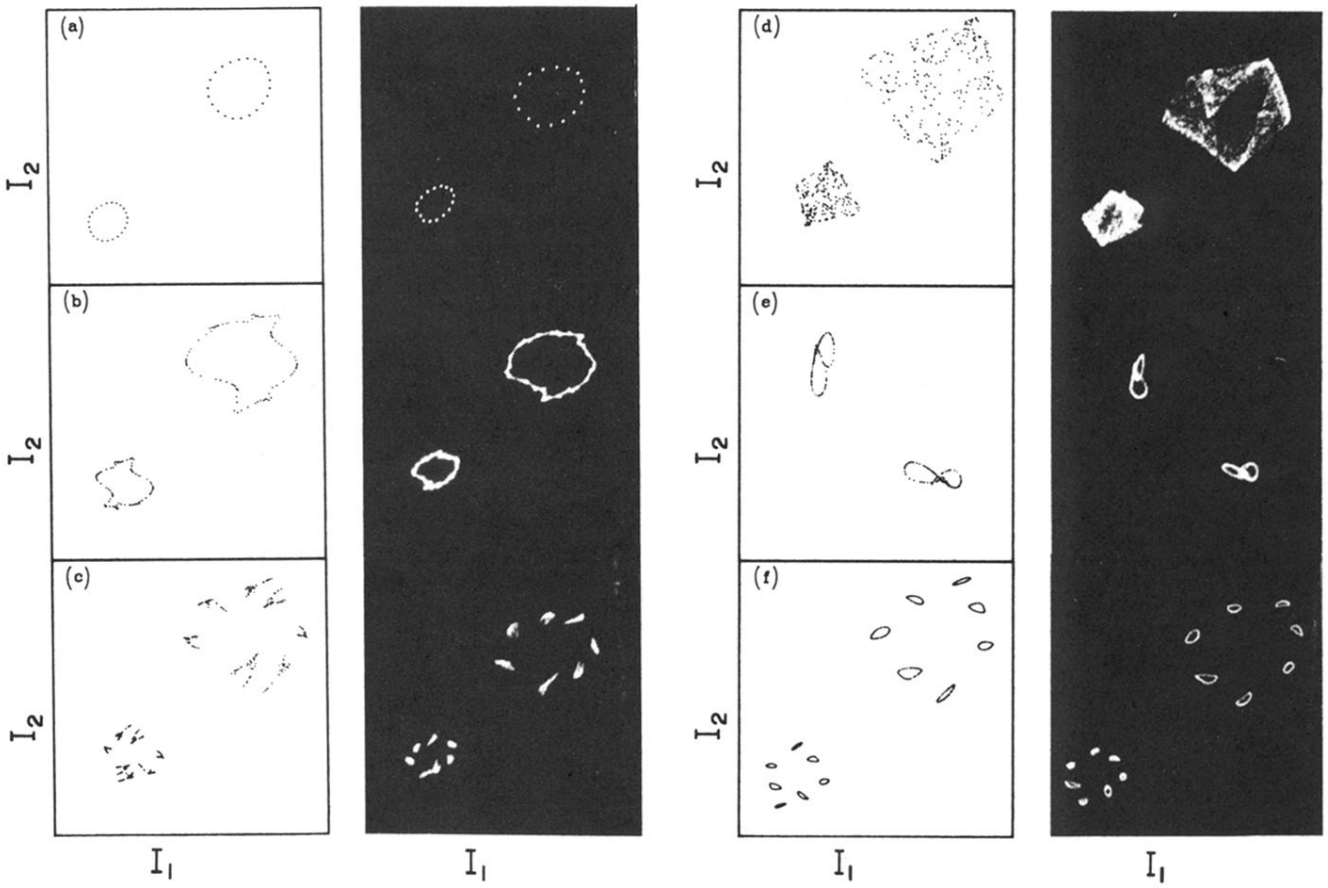

FIG. 3. Corresponding simulated (left) and measured (oscilloscope photographs on the right) Poincaré sections formed by the peak forward currents I_2 vs I_1 (plotted in arbitrary units) for the coupled diode resonator system. The simulations contain 500 calculated points. The drive voltages for the simulation, V_0/V_F, and experimental systems, respectively, were (a) 4.65 and 2.078 V_{rms}, (b) 5.25 and 3.082 V_{rms}, (c) 5.55 and 3.296 V_{rms}, (d) 5.95 and 3.747 V_{rms}, and (e) 6.50 and 4.833 V_{rms}. For (a)–(e), simulation: $\omega/\omega_0=1.30$; measurements: drive frequency, $f=56$ kHz and $R=2940\ \Omega$. For (f) simulation: $\omega/\omega_0=1.27$, $V_0/V_F=5.29$; and measurements: $f=52.4$ kHz, $R=2964\ \Omega$, and $V=4.34$ V_{rms}. All other parameters are constant and given in Sec. III B 1.